APPENDIX A

The Child-Langmuir law

Consider the flow of electrons between two parallel plates, by assuming that the cathode freely emits electrons. The Poisson's equation for space charge with density ρ in one dimension is

$$\nabla^2\Phi = \frac{d^2\Phi}{dx^2} = -\frac{\rho}{\varepsilon_0} = -\frac{en_e}{\varepsilon_0} \tag{A.1}$$

where Φ is the electric potential. The current density may be written

$$J = -en_e(x)v(x) = \text{ const.} \tag{A.2}$$

Assume electrons emitted with velocity = 0 and no collision while travel between plates, energy conserved

$$\frac{1}{2}mv^2 = e\Phi \text{ or } v = \sqrt{\frac{2e\Phi}{m}} \tag{A.3}$$

Solving n_e (A.2) by putting v and substitute to (A.1). One obtain

$$\frac{d^2\Phi}{dx^2} = -\frac{J}{\varepsilon_0\sqrt{\frac{2e\Phi}{m}}} \tag{A.4}$$

to be solved with initial conditions $\frac{d\Phi}{dx} = 0$ and $\Phi = 0$ at x = 0.

The first integration of (A.4), simplified by multiply the left side by $2\frac{d\Phi}{dx}dx$ and the right side by the equivalent $2d\Phi$, leads to

$$\left(\frac{d\Phi}{dx}\right)^2 = \frac{4J}{\varepsilon_0}\sqrt{\frac{m\Phi}{2e}} \tag{A.5}$$

By separation of V and x and the resulting equation can be integrated to yield

$$\Phi = \left(\frac{m}{2e}\right)^{1/3}\left(\frac{J}{\varepsilon_0}\right)\left(\frac{3x}{2}\right)^{4/3} \tag{A.6}$$

Since $\Phi = V$ at $x = d$, we obtain

$$J = \frac{4}{9}\varepsilon_0\sqrt{\frac{2q}{m}}\frac{V^{3/2}}{d^2} \tag{A.7}$$

APPENDIX B

B1) Fortran code to calculate B-field in multicusp ion source

```
dimension r(65),z(65),br(65,65)
  Rmax=0.05
  Zmax=0.09
  dz=Zmax/64
  dr=Rmax/32
DO 5 I=1,65
 R(I)=(I-1)*DR
 Z(I)=(I-1)*DZ
5 CONTINUE
DO 10 I=1,33
 DO 10 J=1,65
10  BR(I,J)=1800*EXP(-200*R(34-I))
  open (1,file='bmag.dat',form='formatted',access='sequential')
 do 15 j=1,65
do 15 i=1,33
15 write (1,*)z(j),r(i),br(i,j),0,0
99 format(e5.4,e5.4,e5.4,i1,i1)
END
```

B2) Data file for Argon plasma simulation: XOOPIC

```
default
{Rfdis}
Region
{
Grid
{
        n2 = 1.000e+00
        x2f = 5.000e-02
        x2s = 0.000e+00
        K = 32
        n1 = 1.000e+00
        x1f = 9.0e-02
        x1s = 0.000e+00
        J = 64
        Geometry = 0
        Rule
        {
        Limit
         n1 < 2.500e-01
         Fatal -- n1 < 0.25 grid spacing too nonuniform to ensure accuracy
        }
}
Control
{
        Bf = bmag.dat
        dt = 3.0e-12
        ElectrostaticFlag = 0
        Rule
        {
        Limit
         dt <= 0.000e+00
         Fatal -- time step must be positive
        }
}
CylindricalAxis
{
        normal = 1
        k2 = 0
        j2 = 64
        k1 = 0
        j1 = 0
}
Conductor
{
        normal = 1
        k2 = 32
        j2 = 0
```

```
        k1 = 0
        j1 = 0
        Secondary
        {
                secondary = 0.1
                secSpecies = electrons
                iSpecies = argon
        }
}
Conductor
{
        normal = -1
        k2 = 32
        j2 = 64
        k1 = 32
        j1 = 0
        Secondary
        {
                secondary = 0.1
                secSpecies = electrons
                iSpecies = argon
        }
}
Conductor
{
        normal = -1
        k2 = 0
        j2 = 64
        k1 = 32
        j1 = 64
        Secondary
        {
                secondary = 0.2
                secSpecies = electrons
                iSpecies = argon
        }
}
Species
{
        name = electrons
        m = 9.11e-31
        q = -1.6e-19
        collisionModel=1
}
Species
{
      name = argon
      m = 6.67e-26
      q = 1.6E-19
        subcycle = 100
        collisionModel=2
}
MCC
```

```
{
        gas = Ar
        pressure = 0.01
        eSpecies = electrons
        iSpecies = argon
}
PortTM
{
        A = 25
        frequency = 1.35e7
        j1 = 36
        j2 = 36
        k1 = 0
        k2 = 16
      name = RF-Coil
        normal = 1
        EFFlag = 1
}
Load
{
        x1MinMKS = 0.000
        x1MaxMKS = 0.09
        x2MinMKS = 0.00
        x2MaxMKS = 0.05
        speciesName = electrons
        density = 1.0e16
        np2c = 1.1E10
        temperature = 5.93e5
}
Load
{
        x1MinMKS = 0.00
        x1MaxMKS = 0.09
        x2MinMKS = 0.00
        x2MaxMKS = 0.05
        speciesName = argon
        density = 1.0e16
        np2c = 1.1E10
        temperature = 4.9e2
}
```

APPENDIX C

The phase ellipse relation

The parameters β, α and γ in 4.4 can be defined by using a generalized ellipse rotated by an arbitary angle ψ (Willie, 2000) as,

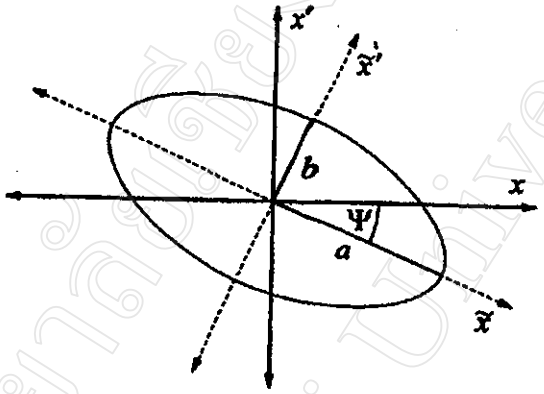

$$\begin{aligned} \beta &\equiv \frac{b}{a}\sin^2\Psi + \frac{a}{b}\cos^2\Psi \\ \alpha &\equiv \left(\frac{a}{b} - \frac{b}{a}\right)\cos\Psi\sin\Psi \\ \gamma &\equiv \frac{b}{a}\cos^2\Psi + \frac{a}{b}\sin^2\Psi \end{aligned} \qquad \text{(C.1)}$$

where a is ellipse major axis, b is ellipse minor axis. Using the expression for the ellipse area $A = \pi ab$, the general equation of an ellipse is then given by

$$\frac{A}{\pi} = \beta x'^2 + 2\alpha x x' + \gamma x^2 = \varepsilon \qquad \text{(C.2)}$$

The ellipse is thus uniquely defined by the parameters β, α, γ and ε. The points of intersection with the coordinate axes are obtained by setting $= 0$ or $x' = 0$, namely

$$\begin{aligned} x &= \sqrt{\frac{\varepsilon}{\gamma}} \qquad \text{for} \quad x' = 0 \\ x' &= \sqrt{\frac{\varepsilon}{\beta}} \qquad \text{for} \quad x = 0 \end{aligned} \qquad \text{(B.3)}$$

APPENDIX D

Papers by author

D1 Paper I: A 13.56 MHz multicusp ion source for high intensity Ar beam, *Rev. Sci. Instrum. 71(2)* 1181 2000.

D2 Paper II: Plasma emission in vacuum arc and RF-discharge plasma source, *Rev. Sci. Instrum.* 73(2) 754 2000.

D3 Paper III: Characteristics of a 13.56 MHz radiofrequency driven multicusp ion source, submitted for publication in *Plasma Sources Science and Technology.*

A 13.56 MHz multicusp ion source for high intensity Ar beam

D. Boonyawan,[a] N. Chirapatpimol, N. Sanguansak, and T. Vilaithong
Department of Physics, Fast Neutron Research Facility, Faculty of Science, Chiang Mai University, Chiang Mai 50200, Thailand

(Presented on 9 September 1999)

A 13.56 MHz radio frequency (rf) inductively coupled multicusp ion source has been developed for producing an intense argon beam with current density in excess of 30 mA cm^{-2}. The source chamber is a 10 cm diam aluminum cylinder surrounded by 20 rows of 3.5 kG Sm–Co_5 magnets which form a longitudinal line-cusp field configuration. The rf antenna coil, placed inside the source chamber, is made of a braided wire threaded through a two turn pyrex tube 6 cm in diameter to prevent electrical leakage and ion sputtering. A 10:1 turns-ratio matching transformer is used to match the 50 Ω output impedance of the rf generator to the impedance of the plasma load. Preliminary measurements were carried out with a single- and four-hole aperture extracting system using argon gas. For single-hole extraction with pressure at 5 mTorr and rf power at 500 W, the ion current density was 27 mA cm^{-2}. Under the same operating condition, a four-hole extracting system could achieve almost the same amount of current density of 25 mA cm^{-2}. © *2000 American Institute of Physics.* [S0034-6748(00)68402-2]

I. INTRODUCTION

A radio-frequency (rf) driven multicusp ion source has been developed for applications that need a large volume of uniform, high density, and quiescent plasmas.[1–5] The cusp field attains a uniform plasma density distribution in the source because primary electrons always diffuse back into the center. Furthermore, the plasma is free from high-energy electrons because of electron–neutral particle collisions arising from the drift motion in the cusp field. The rf discharge plasma has several advantages over the dc filament discharge because of its simpler structure, longer lifetime of operation, and no filament contamination on the target, even in the high power continuous wave (cw) mode.[1,5,6] The rf inductively coupled technique has been shown to give an ion beam with much less energy spread than that of a capacitively coupled one.[5,7] Also, it has a higher discharge efficiency, especially when operated in cooperation with a multicusp magnetic field.[1,8] An earlier version of the rf discharge plasma source with multicusp permanent magnet confinement developed at Chiang Mai University has been successful in the production of an ion beam from reactive gas such as oxygen.[9]

This article describes a modified version of our 13.56 MHz multicusp ion source for the production of an intense argon beam using a multihole ring beam extracting system.

II. EXPERIMENT

A. Ion source

The ion source which is an improved version of the CMU 13.56 MHz multicusp ion source described previously[9] is shown schematically in Fig. 1. The source chamber is made of an anodized aluminum cylinder 10 cm in diameter and 9 cm long. The inner wall is surrounded by 20 columns of Sm–Co_5 magnets to form a longitudinal line-cusp field configuration. The plasma is produced by an inductively coupled rf discharge, in which rf power is transferred by ohmic dissipation of induced rf currents which are caused to flow in the plasma by high frequency transformer action. The rf power is fed to an antenna coil placed in the ion source chamber via a tunable matching box.

The new rf antenna coil is made of a braided wire threaded through a two-turn pyrex tube bent in a circular shape 6 cm in diameter. This version of the rf antenna coil has been adopted to avoid cracks in the porcelain coating due to the thermal stress founded in the last coil version. The advantage of using a braided wire in place of a single tube is that it increases the surface of conducting rf current in addition to easing the threading process.

The matching box, as shown in Fig. 2, is installed with rf shielding and electrically connected to the end flange of the ion source to reduce rf coupling to the extraction voltage. A

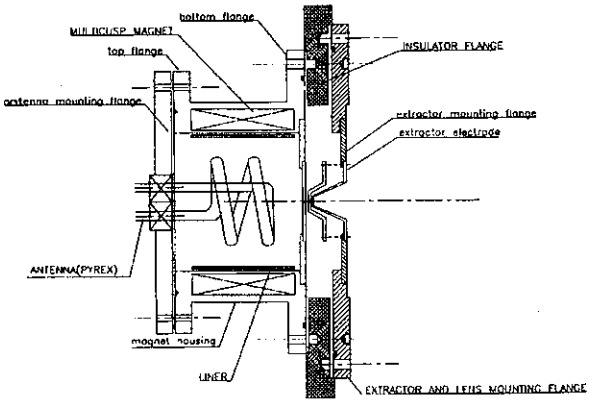

FIG. 1. Schematic diagram of the CMU 13.56 MHz multicusp ion source.

[a]Author to whom correspondence should be addressed; electronic mail: dherawan@science.cmu.ac.th

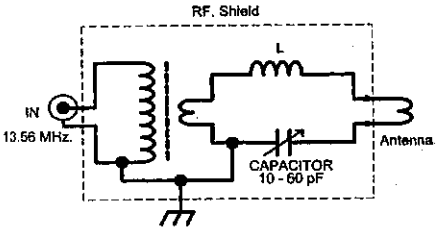

FIG. 2. Matching circuit for maximum rf power transfer to the antenna coil.

10:1 turns-ratio matching transformer steps up the load current while the capacitor C and inductor L keep the matching resonance at 13.56 MHz. rf filters are used at all input and output connectors to suppress all possible rf interferences that may affect the measured signal.

B. Beam extraction

Normally, the process of extracting and transporting the positive ion beam with high current density relies on electrical neutralization of the beam by low energy electrons to keep it from expanding under the influence of its own space charge. Recently, other techniques such as the aperture displacement technique[10] and dished grid extraction[11] have been tried for an intense ion beam. We have choosen the multihole aperture with the quasi-Pierce type electrode approach.

Two types of extraction systems have been used for the experiments. One is a single-hole three-electrode extraction system, which includes three stainless-steel electrodes with a 2 mm diam hole. The electrode spacings are 3 and 1 mm, respectively. The other is a multihole extraction system, which is made of three stainless steel dishes with four of 2 mm extraction holes situated on the 2.4 cm diam circle to produce a (discrete) ring beam. With this configuration, the second electrode for both types of extractions operates as a suppressor to prevent backstreaming electrons from accelerating back to the ion source.

Experiments have been carried out on a T-shaped vacuum chamber test bench with a 520 $\ell\,s^{-1}$ turbomolecular pump. The ion source is powered by a 1250 W transistorized 13.56 MHz rf generator (ENI-OEM-12A) via a matching box. Extraction and suppression voltage supplies cover the range of 0–30 kV and 0–−5 kV (Glassman HV Inc.), respectively. The gas supply is controlled by a precision needle valve. Closed-circuit cooling water with adequate flow rate is supplied to all devices.

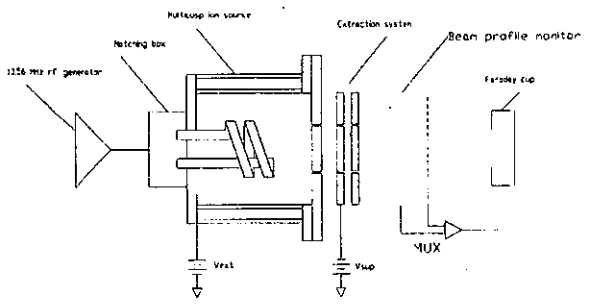

FIG. 3. Schematic of the experimental setup.

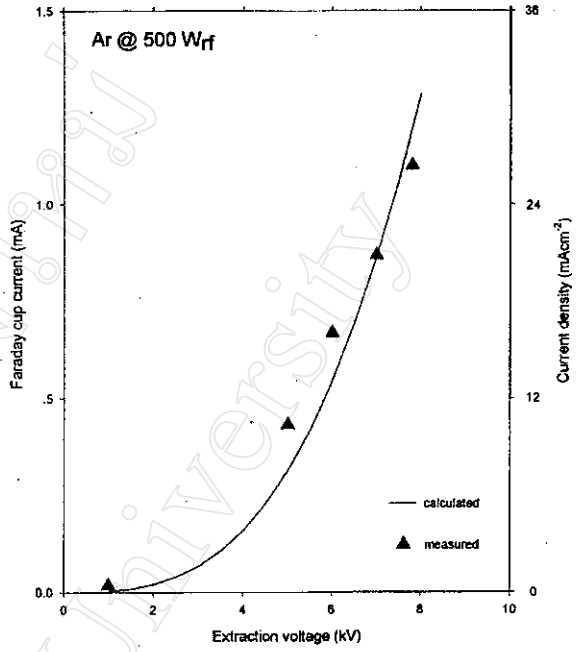

FIG. 4. Argon current density vs extraction voltage at 500 W rf power from single hole extraction. Solid line is calculated from the Child–Langmuir equation.

The experimental arrangement including the ion source, the extraction system, and a Faraday cup is shown in Fig. 3. Typically, the first extraction or plasma electrode is electrically biased at 5 kV, and the second electrode at −1 kV with

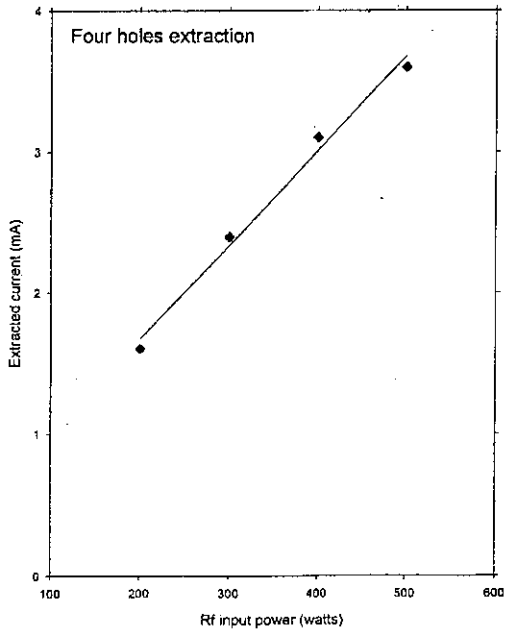

FIG. 5. Extracted argon current vs rf input power from four-hole extraction.

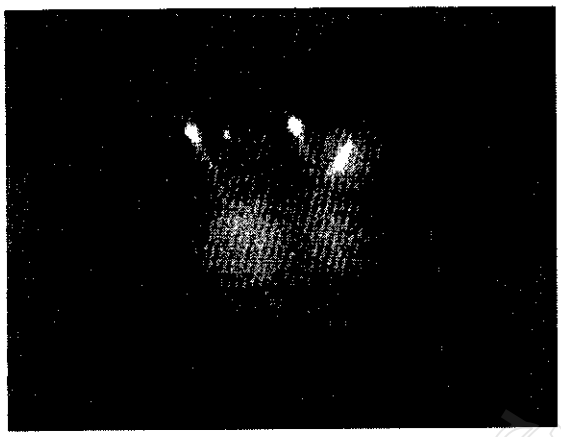

FIG. 6. Image of the four argon beam spots as seen on the beam profile monitor.

respect to ground, while the third one is connected to ground. The operating pressure of argon gas is 5 mTorr unless specified. The Faraday cup is made from stainless steel and biased with -120 V to suppress the secondary electron emission. The rf power supply is installed on an isolation stand to operate at the same potential as the ion source. This rf arrangement has been founded[3] to reduce the ion beam energy spread due to rf interference. The current density is obtained by dividing the extracted beam current by the total beam extraction area.

III. RESULTS

Figure 4 shows the dependence of the argon current density against extraction voltage at 500 W rf power from the single-hole extraction system. The saturation current density of 27 mA cm^{-2} is realized at about 8 kV extraction voltage. The extracted beam current almost follows the Child–Langmuir equation. For this extraction geometry, the angle of beam divergence measured by two sets of the multiwire beam profile monitor is found to be about 49 mrad. The experiment indicates that the argon current increases with the decrease in source pressure and increases linearly with increasing rf power. Figure 5 shows the extractable argon current as a function of rf power from the four-hole extraction system. The argon current measured by the modified Faraday cup for this large beam is about 3.4 mA. Figure 6 shows four argon beam spots on the beam profile monitor with average current density of about 25 mA cm^{-2}.

IV. CONCLUSIONS

We have constructed a high intensity argon ion source producing a ring beam with a four-hole, three-electrode extraction system. Our experimental results obtained thus far indicate that for this kind of ion source, the current–power relation at this discharge frequency and maximum argon current density obtained are in agreement with other experiments[5,6,9,12] at 40 mA cm^{-2}kW^{-1}. We plan to increase beam brightness by increasing the number of extracting holes and optimizing the extraction system geometry.

ACKNOWLEDGMENTS

The authors would like to thank W. Tantraporn for his technical advice and encouragement and K. N. Leung for his advice on the design of the first version of this ion source. They also thank R. Chareonnukul, S. Amkaew, and N. Pasaja for their technical assistance. This work is supported in part by the Thai Research Fund.

[1] K. N. Leung, D. A. Bachman, P. R. Herz, and D. S. McDonald, Nucl. Instrum. Methods Phys. Res. B **74**, 291 (1993).
[2] P. Spadtke, J. Bossler, H. Emig, K. D. Leible, C. Muhle, H. Reich, H. Schulte, and K. Tinschert, Rev. Sci. Instrum. **69**, 1079 (1998).
[3] W. A. Barletta, W. T. Chu, and K. N. Leung, Rev. Sci. Instrum. **69**, 1085 (1998).
[4] Y. Lee, R. A. Gough, W. B. Kunkel, K. N. Leung, J. Vujic, M. D. Williams, D. Wutte, and N. Zahir, Rev. Sci. Instrum. **69**, 877 (1998).
[5] D. Wutte *et al.* Nucl. Instrum. Methods Phys. Res. B **142**, 409 (1998).
[6] S. T. Melnychuk, T. W. Deblak, and J. J. Sredniawski, Rev. Sci. Instrum. **67**, 1662 (1996).
[7] Y. Lee *et al.* Rev. Sci. Instrum. **68**, 1398 (1997).
[8] T. Shirakawa, H. Toyoda, and H. Sugai, Jpn. J. Appl. Phys., Part 1 **29**, 1015 (1990).
[9] D. Boonyawan, P. Suanpoot, and T. Vilaithong, Surf. Coat. Technol. **112**, 314 (1999).
[10] H. Oguri, Y. Okumura, N. Miyamoto, J. Kusano, and M. Mizumoto, Rev. Sci. Instrum. **67**, 1051 (1996).
[11] J. Freisinger, J. Krempel-Hesse, J. Krumeich, H. Lob, W. D. Munz, and A. Scharmann, Rev. Sci. Instrum. **63**, 2441 (1992).
[12] K. N. Leung, in "Ion Source for High Purity Ions," *Proceedings of Application of Accelerators in Research and Industry*, edited by J. L. Duggan and I. L. Morgan (AIP, New York, 1997), pp 1203–1205.

REVIEW OF SCIENTIFIC INSTRUMENTS VOLUME 73, NUMBER 2 FEBRUARY 2002

Plasma emission in vacuum arc and rf-discharge plasma sources

D. Boonyawan, S. Davydov,[a] B. Yotsombat, N. Chirapatpimol, and T. Vilaithong
Fast Neutron Research Facility, Department of Physics, Faculty of Science, Chiangmai University, Chiangmai 50200, Thailand

(Presented on 4 September 2001)

Optical emission spectra from plasma produced by a copper vacuum arc with argon and nitrogen have been investigated for the case when the plasma was guided by a straight solenoid. The spectra have been compared with those obtained from inductively coupled rf multicusp discharge in the 10^{-4}–10^{-2} Torr argon and nitrogen pressure range and at an input power of up to 500 W. It has been found that the spectral line intensity distributions of neutral and ion species for arc and rf discharge were different. Also, the intensity evolutions of the lines have shown a different behavior between the arc current and rf power. Electron excitation temperature (T_{ex}) for rf argon plasma at low pressure has been found to be approximately 2.5 eV which was about ten times higher than for Cu-argon arc discharge. Possible mechanisms of ionization-excitation of guest atoms/molecules in the case of metal vacuum arc discharge are discussed. © *2002 American Institute of Physics.*
[DOI: 10.1063/1.1429780]

I. INTRODUCTION

Vacuum arc (VA) and inductively coupled rf plasma sources are of great interest for plasma immersion ion implantation and deposition. Besides single component pure metal ion or gaseous ion species, more complicated mixtures of gases such as N_2, O_2, methane, and acetylene are now used in VA and rf discharges to produce nitride and oxide metal coatings, diamondlike carbon films, etc.[1] In these cases, optical emission spectroscopy (OES) becomes an especially efficient diagnostic tool for investigations of plasma characteristics. Conventional probe techniques can only supply information about integration current for all ion species and charge states. For a pure copper vapor vacuum arc discharge the emission spectra of plasmas have been described elsewhere.[2,3] Here we present the OES data for our VA plasma source with a copper cathode in the case of admixture into a vacuum chamber of Ar and N_2 gases in comparison with spectral data obtained from inductively coupled rf plasma source for wide ranges of Ar and N_2 pressure and rf power.

II. EXPERIMENTS

The schematic diagrams of the experimental facilities are shown in Fig. 1. The VA source consists of an 8 mm diameter copper cathode and stainless steel ring-shaped trigger electrode insulated by a Pyrex tube with a 1 mm wall thickness. An aluminum tube with an inner diameter of 30 mm serves as the anode. The cathode and anode holders are water-cooled. The source is attached to a cylindrical vacuum chamber approximately 0.22 m^3 in volume. The 40 cm length straight solenoid with an inner diameter of 30 mm made from 2.5 mm diameter copper wire was electrically connected in series with the anode. An LC line (1.4 Ω impedance) produced arc currents of up to 400 A with a pulse duration of about 0.6 ms.

The rf discharge plasma source is a modified CMU 13.56 MHz multicusp source.[4] The source housing was made of a stainless steel cylinder 10 cm in diameter and 9 cm long. The inner wall is surrounded by 20 columns of Nd–Fe–B magnets to form a longitudinal line-cusp field configuration. The rf power is transferred via an L-C matching box directly coupled to the plasma by a rf antenna immersed inside the source chamber. The antenna coil is made of a braided copper wire threaded through a two-turn quartz tube wound with a 6 cm diameter.

Optical emission from pure copper arc discharges and copper with argon or nitrogen could be monitored along the solenoid axis or in the off-axis direction. Spectra were recorded via a 2-m-length fiber optic cable with UV collimating lens through quartz window view-ports by an Ocean Optics S2000 Fiber Optic Spectrometer (model I2J1353). Also, an additional quartz lens with a 30 mm focal length was placed close to the windows. The wavelength dependence of the sensitivity of the spectrometer has been corrected with the help of the HgAr calibration light source.[5] The spectral resolution was about 0.6 nm. An integration time of 2 s was used to record the emission spectra in a single-pulse mode operation of VA source and was varied from 0.1 to 10 s for the rf plasma source. The residual gas pressure before VA source operation was usually 8×10^{-6} Torr and Ar or N_2 were added for a pressure of up to 6×10^{-4} Torr.

III. RESULTS

Optical emission spectra in the range of 400–550 nm from argon rf plasma and copper arc plasma mixed with argon are shown in Fig. 2. In this spectral range the more intensive lines of singly ionized Ar atoms were observed. The spectra have been normalized to the peak intensity of the

[a]Institute for Science and Technology Research and Development, Chiangmai University, Chiangmai 50200, Thailand.

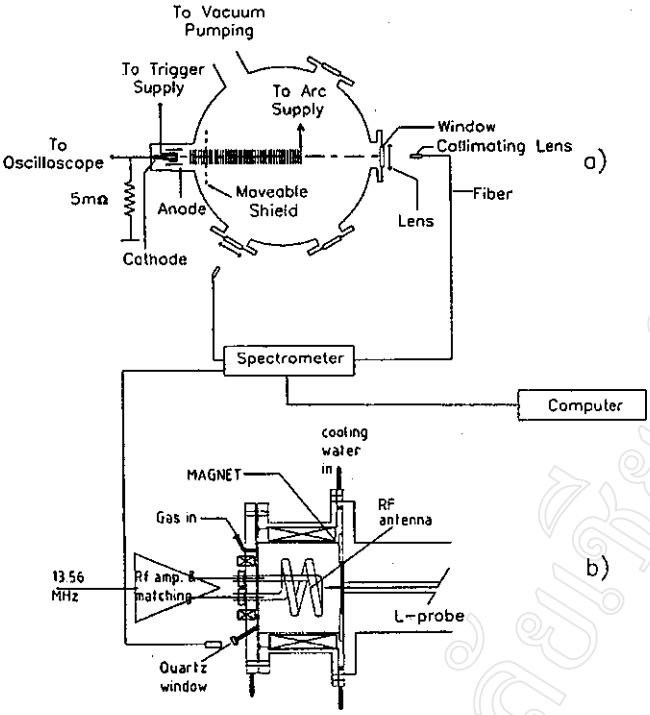

FIG. 1. Schematic diagrams of experimental facilities: (a) VA plasma source and (b) rf plasma source.

line at 488 nm belonging to Ar^+. One can see that the spectra differ. In the case of the rf discharge the intensities of the lines belonging to exited neutral atomic species are higher than for ion species, especially at high pressure. For copper arc plasma mixed with Ar the relative spectral intensity distribution of the lines is contrary to the case of rf plasma; the intensity of the lines belonging to the exited neutral Ar are much lower than the intensity of Ar^+ lines. In fact, only ion lines can be observed. Similar comparison of emission spectra from rf N_2 discharge and copper mixed with N_2 arc discharge is presented in Fig. 3. In this figure we normalize the spectral lines to the peak intensity of the line at 391.5 nm belonging to N_2^+. It can be seen that in the case of low pressure the relative intensity distribution of the lines belonging to N_2 and N_2^+ is almost identical for both discharges except that for the arc discharge, the transitions in the first positive band of N_2 are not observed (two most intensive lines observed at 324.7 and 327.4 nm belong to neutral Cu atoms). In the case of higher nitrogen pressure in rf plasma the intensities of lines belonging to the neutral N_2 species increase more strongly relative to N_2^+ lines.

Figure 4(a) shows the evolution of intensities of some spectral lines corresponding to excited neutral Cu (324.7 nm) and N_2 (337.1 and 380.5 nm) species and N_2^+ ions (391.4 and 427.8 nm) versus arc discharge current. The intensity evolution of N_2 and N_2^+ lines for rf discharge is shown in Fig. 4(b). One can see that the intensity of the line belonging to Cu is proportional to the arc current. (Note that similar linear dependences of intensities versus arc current have been observed also for many other spectral lines belonging to different excited Cu, Cu^+, and Cu^{++} species.[3]) At the same time, the intensity evolution of N_2 and N_2^+ lines show saturation at high arc current. In the case of rf discharge below 500 W the

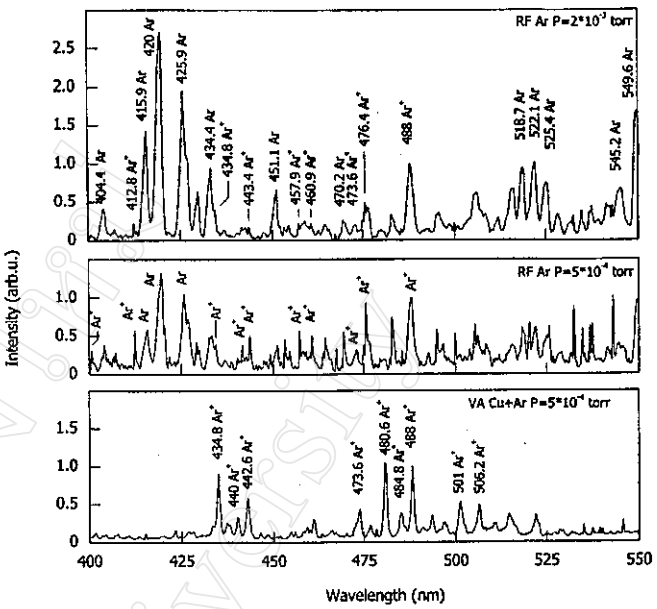

FIG. 2. Emission spectra from argon rf plasma at low and high pressures and copper arc plasma mixed with argon.

intensities of the same N_2 and N_2^+ lines do not lead to saturation with increasing rf power. In the range of 300–400 W the intensities of the lines rapidly increase showing "intensity jump." This jump corresponds to the known phenomena of mode change from the capacitive to the inductive discharge when the power exceeds the threshold level. The density of electrons rapidly increases 50–100 times more in the inductive discharge mode, as observed by Langmuir probe measurement,[6] which is in good agreement with our spectroscopy measurement. Thus, the intensity jump was found to be almost 100 times for all atomic and molecular spectral lines.

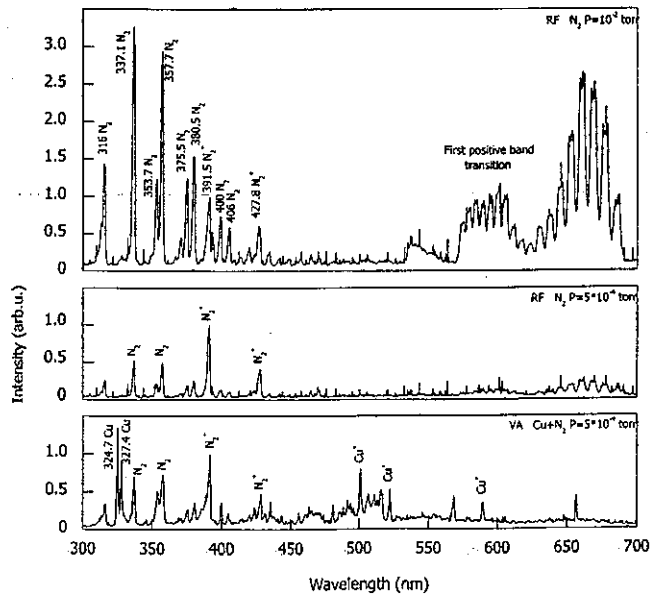

FIG. 3. Emission spectra from N_2 rf plasma at low and high pressures and copper arc plasma mixed with N_2.

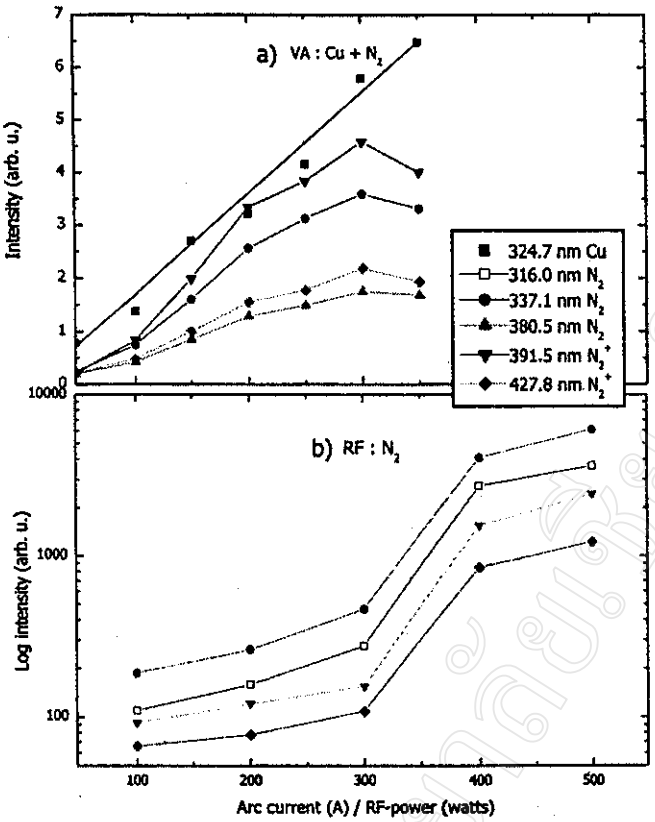

FIG. 4. Intensity evolutions of spectral lines versus arc current (a) for Cu–N_2 and rf power (b) for N_2 discharges.

IV. DISCUSSIONS

In the case of rf discharge the difference of spectral line intensity distribution observed at different pressures of Ar and N_2 could in general be explained in terms of mean electron temperatures. We have measured electron ionization T_{in} and excitation T_{ex} temperatures at different argon pressures. In Fig. 5, T_{in} was measured by a Langmuir probe whereas T_{ex} was measured by the method of relative intensities of spectral lines.[7] The following lines, belonging to neutral excited Ar atoms, have been chosen: 394.9, 404.4, 415.9, 420.07, 425.9, 427.2, 451.07, 549.6, 555.9, 560.7, and 641.6 nm. The data of the transition probabilities, statistical weights, and energies of upper levels were taken from Refs. 8 and 9. It is seen that even in the relatively narrow pressure range from 2 to 10×10^{-3} Torr, T_{in} and T_{ex} decrease by about 25% with increasing gas pressure. Also, the value of T_{ex} is about 20% lower than T_{in} which agree with the literature data.[10] Note that at difference pressures T_{in} was almost constant in the range between 50 and 500 W of rf power. From Fig. 4(b) one can assume that the T_{ex} of rf discharge is slightly dependent on rf power. This assumption is justified because, for neutral and ion species, the slope of each lines follows similar pattern when the discharge mode changes.

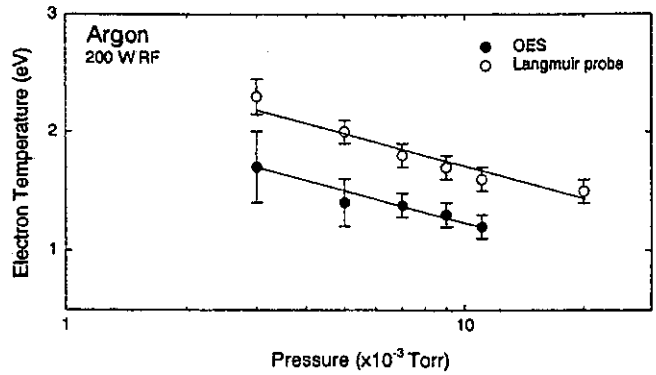

FIG. 5. Electron temperature as a function of argon pressure in rf discharge measured by Langmuir probe (top) and OES methods (bottom).

In the case of VA discharge the mechanism of excitation and ionization of guest atoms or molecules is not obvious. The direct collisional electron impact excitation-ionization processes are low. This is probably because the plasma inside of the magnetic duct at long distances from the cathode is cooled due to adiabatic expansion in vacuum. Electrons heating by induced electric fields during the rise time of arc current pulse is not probable. To test this assumption we blocked a part of the plasma beam by nontransparent dielectric shield, as shown in Fig. 1(a). There was no emission from Ar behind the shield. The photon re-absorption processes should be ruled out because the spectra recorded along the solenoid axis and in the off-axis directions were similar. Also, the efficiency of ionization by direct vacuum ultraviolet photon radiation should be negligible at such low argon pressure. We suppose that the most probable mechanism of Ar ionization in the Cu+Ar arc discharge is the resonant charge transfer $Cu^+ + Ar \rightarrow Cu + Ar^+$. These type of reactions are known to have a high cross section, especially, at ion kinetic energies about 20 eV which normally takes place in VA discharges.[1] Furthermore, Cu ions have several sets of metastable levels with the energy approximately between 15 and 17 eV ($4f$, $4d$, $5p$, and $6s$)[11] that are almost in resonance with the ionization potential of Ar (15.76 eV). This mechanism can also play the important role in the excitation-ionization processes of N_2 molecules (ionization potential of N_2 is approximately 15.5 eV). Additional process of increasing the emission from neutral N_2 can occur due to the two-body recombination: $e + N_2^+ \rightarrow N_2 + h\nu$.

ACKNOWLEDGMENTS

The authors would like to thank N. Pussadee and P. Poolcharoensilp for their technical assistance. This work is partly supported by the Thai Research Fund.

[1] A. Anders, *Handbook of Plasma Immersion Ion Implantation and Deposition* (Wiley, New York, 2000).
[2] A. Anders and S. Anders, J. Phys. D **24**, 1986 (1991).
[3] B. Yotsombat, S. Davydov, T. Vilaithong, P. Poolcharuansin, and I. G. Brown, J. Phys. D **34**, 1928 (2001).
[4] D. Boonyawan, P. Suanpoot, and T. Vilaithong, Surf. Coat. Technol. **112**, 314 (2000).
[5] M. W. Rhodes, S. Wanwilairat, T. Vilaithong, and W. Hoffmann, Rev. Sci. Instrum. **71**, 2053 (2000).
[6] K. Suzuki, K. Nakamura, H. Ohkubo, and H. Sugai, Plasma Sources Sci. Technol. **7**, 13 (1998).
[7] A. Montaser and D. W. Golightly, *Inductively Coupled Plasma in Analytical Atomic Spectroscopy* (VCH, New York, 1987).
[8] D. R. Lide, *Handbook of Chemistry and Physics* (CRC Press, Boca Raton, 1994).
[9] NIST, *Atomic Spectra Database Lines Data* (http://physics.nist.gov).
[10] M. A. Liberman and A. J. Lichtenberg, *Principles of Plasma Discharges and Materials Processing* (Wiley, New York, 1994).
[11] C. E. Little, *Metal Vapour Lasers* (Wiley, Chichester, 1999).

Characteristics of a 13.56 MHz radiofrequency driven multicusp ion source

D. Boonyawan, N. Chiraphatpimol and T.Vilaithong

Fast Neutron Research Facility, Department of Physics, Faculty of Science, Chiang Mai University, Chiang Mai 50200, Thailand

Abstract

*The characteristics of a radiofrequency (rf) driven multicusp ion source are investigated. The ion source is a Nd-Fe-B magnetic multicusp type operated at 13.56 MHz with an internal quartz covered antenna. Simulation of inductive discharge of Argon is performed using two-dimensional relativistic electromagnetic particle-in-cell code XOOPIC (Verboncoeur et al 1995 Comp. Phys. Comm. **87** 199). The source has been diagnosed by an rf compensated Langmuir probe for uniformity, density and electron temperature. A retarding field energy analyser, and a multi-wire beam profile monitor and quadrupole magnet system have been used for beam energy spread and emittance measurements. Experiments were performed with Argon gas and rf power up to 500 W. A plasma density of up to 1.5 x 10^{18} m^{-3} was obtained. The rms beam emittance is found to be about 32 +/- 4 mm mrad and the energy spread of the Argon beam is around 3.1 +/- 0.5 eV at 3 kV extraction. The rf coupling to the extracting voltage could be suppressed by a 1.2 mH rf-choke which results in the reduction of the axial energy spread in the extracted beam.*

1. Introduction

Because of their ability to produce a quiescent and high density plasma with good performance in electrical and gas efficiencies, multicusp ion sources have been widely studied for applications in ion implantation, microlithography, and nuclear science experiments [1-4]. Multicusp plasma source using permanent magnets was first reported by Limpaecher and MacKenzie[5]. Leung *et al* [6] performed an experiment to optimize permanent magnet geometries and found the full line cusp to give optimum plasma density. Characteristics of a steady-state, dc discharge multipole ion source was subsequently reported [7]. In recent years an rf driven ion source has attracted great interest over filament-discharge because of its simpler structure, longer operational lifetime and clean plasma discharge [8]. The only disadvantage of an rf driven source is its large energy spread on both axes due to an rf coupling to the grid extracting voltage which were found in some experiments [9-10]. A 13.56 MHz rf plasma was mainly used in inductively coupled plasma (ICP) applications. Furthermore, an inductively coupled rf discharge in multipole fields could maintain a uniform large volume plasma at very low neutral pressure [11-12]. This type of discharge is competitive with both magnetron and ECR-type plasmas for low pressure etching or deposition processes [11]. In the interest of plasma applications, several rf inductively modeling studies [13-20] have been made on frequency, skin depth, gas type, internal and external discharge and E-H mode jump with reasonably good agreement with data obtained from measurements. As for ion source application, a 13.56 MHz inductively coupled internally discharged or so called rf driven source has been studied extensively recently by a group at the Lawrence Berkeley National Laboratory [3,21-23] and elsewhere [24-26]. Lee *et*

al [23] operated their 10 cm diameter and 10 cm long rf driven multicusp ion source with a maximum output power of 2.5 kW. Their rf antenna was made of copper tubing and coated with a thin layer of porcelain. The external surface of the source chamber was surrounded by 20 columns of Samarium-Cobalt permanent magnets. They measured the axial ion energy spread to be approximately 3.2 eV and found that the extractable beam current was comparable to that of a filament discharge source. They were able to reduce the axial energy spread considerably by installing the rf power supply on the high voltage platform and shielding the leads between the matching network, antenna and connecting capacitors for the source chamber to ground. Wutte *et al* [2] reported the development of a similar type of ion source for radioactive ion beam (RIB) application. Their ion sources performance showed promising features for RIB production with a gas efficiency of up to 60 % for Argon and up to 80 % for Xenon and a relatively low axial energy spread of 4-7 eV for the rf driven source.

More recently, filament-discharge multicusp ion sources have been investigated for application in projection lithography [25,26] and focused ion beam [27]. Our interest lies in the micromilling of silicon substrate and gemstones. For this reason, we have investigated the possibility of modifying an rf multicusp ion source for ion milling application. Even though filament-discharge produces a beam with lower axial energy spread [2], we believe rf discharge may be able to compete for long term and clean operation. Argon was chosen for generating discharge plasma because of its high sputtering yield. In this paper, we report comprehensive studies on the performance of the rf driven multicusp ion source which includes some improved features such as the use of Nd-Fe-B type permanent magnet in place of an expensive $Sm\text{-}Co_5$ magnet and the replacement of a high voltage capacitor as used by Lee *et al* [23] with a cascade rf-choke to reduce the modulation of the dc acceleration voltage by rf interference. In section 2, we describe our experimental apparatus and experimental set up. Details of plasma simulation using a particle-in-cell (PIC) computer code are presented in section 3. Results are discussed and concluded in section 4 and section 5.

2. *Experimental apparatus and methods*

2.1 Ion source design

The rf-discharge ion source used in this experiment is a modified version of the CMU 13.56 MHz multicusp ion source described elsewhere [24]. The plasma generated through an inductively coupled rf discharge is excited in electric fields generated by a transformer effect from a rf current in a coil. The changing magnetic field of the coil induces an azimuthal electric field in which the plasma electrons are accelerated. In other words, the rf power is transferred by ohmic dissipation of induced rf currents which are caused to flow in the plasma by high frequency transformer action. The rf power absorbed is given by [28]

$$P_{abs} = \frac{1}{2}\frac{J_\theta^2}{e^2 n_s} m\nu\delta_p, \qquad (1)$$

where J_θ is the amplitude of the induced rf current density, ν is the sum of the collisional and stochastic collision frequency. The collisionless skin depth for the $\nu << \omega_{rf}$ regime can be calculated from [28]

$$\delta_p = \left(\frac{m}{e^2 \mu_0 n_s} \right)^{1/2}, \qquad (2)$$

where n_s is the number of electron in a rf-sheath. In the case of low base pressure, maximum power transfer efficiency occurs when δ_p is approximately equal to the chamber size. A skin depth layer of thickness 2-4 cm has been reported [15] for Argon pressure below 10 mTorr with electron density in the 10^{10}-10^{12} cm^{-3} range. As known, the larger thickness means higher rf to plasma power transfer efficiency. It was also found that for plasma generation in the case of immersed coil, power transfer efficiency is much enhanced [19]. However, as P_{abs} inversely depends on n_s (1), this leads to poor power absorption at high density which results in higher reflected rf power. For very low and very high density discharges, the power transfer could simply be understood as the well-known property of a transformer with an open and a shorted secondary winding, respectively. Parameters such as rf frequency, chamber size, operating pressure are interrelated and have to be taken into account when optimizing the plasma discharge efficiency.

The density of a plasma is dictated by the balance between production and loss processes, with the added restriction to maintain neutrality between ion charge and electron charge. That is to say, it depends on a balance between ionization source distribution and diffusion plasma losses. Energetic electrons, which are useful for ionisation, are more easily lost to the chamber walls than slower ions unless steps are taken to convert fast electrons to plasma. It would also be of advantage to allow slow electron with less than the minimum ionisation energy to escape thus reducing the possibility of electron-ion recombination. By using the multicusp field one is able to confine primary electrons. The alternating rows of permanent magnets generate a line cusp magnetic configuration in which the magnetic field strength B is maximum near the magnets and decays exponentially with distance to the middle of the chamber. Most of the plasma volume is therefore confined in the magnetic field free region. A strong field that exists near the chamber wall will inhibit plasma loss and lead to an increase in plasma density and uniformity. For an alternate pole configuration, the field strength at any point *(x,y)* between two magnets is given by [28]

$$B(x,y) = \frac{2B_0\Delta}{d} e^{-\pi y/d}, \qquad (3)$$

where Δ is the magnet width, d is the magnets separation and B_0 is the residual field strength of the magnet. The field decreases exponentially along the direction into the discharge chamber (y-direction) with decay length d/π independently of x. The magnetic field is zero between magnets and reaches a maximum when y is about $0.28d$. The electron density in a low-pressure plasma could be increased at least by a factor of two with this field configuration whereas an average increase in plasma density by a factor of 30-80 has been reported [29]. An improvement in plasma uniformity follows because diffusion of plasma is inhibited in the strong magnetic field region. Thus, plasma density gradient occurs mostly at the edge, where the diffusion coefficient is small, leading to uniform plasma distribution in the whole region. A uniformity of about 2.5 % is found in a general multipole plasma chamber [28].

We estimated the desired field free region in the ion source by using a 3-D magnetic calculation code called MAGNUS [30]. Its purpose is to solve problems of non-linear magnetostatics in three dimensions to determine magnetic field, energy and flux by using a finite element method. MAGNUS includes 3 processors working as a pre-processor, solver and post-processor such as KUBIK to generate the magnetic mesh points, MAGNUS to solve magnetostatics fields for each mesh point within the boundaries and EPILOG to plot the output value. The version we used was written in FORTRAN 77 which runs on the UNIX platform.

2.2 Extraction system

The transport of the ion beam from a plasma source requires an appropriate extracting system. Design of such a system starts with the desired beam current and energy (I,V), plasma current density (j) and mass of the ion. For our case, only single circular apertures and triode (accel-decel) system will be considered. For circular apertures, the Child-Langmuir beam perveance [31] that characterizes the optics is defined by

$$P_0 = I/V^{3/2} = 1.7\times10^{-7}(Z/A)^{1/2}(a/d)^2AV^{-3/2}, \quad (4)$$

where V is the extracting voltage across the gap d, a is the aperture radius and Z/A is the charge to mass ratio. For minimum divergence, it has been suggested that the optimum perveance should be around $0.45P_0$ to $0.5P_0$ [31]. There are other factors which constrain the design. One of them is the maximum operating voltage in the gap given by

$$V_b = kd^{1/2}, \quad (5)$$

where d is in cm, and a suitable k for Argon is 5×10^4 [31]. The other is the condition to obtain a good beam optics in this system so that the gap d should be greater than or equal to twice the aperture radius a. We chose d to be 4a.

To simulate the beam extraction and transport, a 3-D code called KOBRA3-INP [32] was used. The code KOBRA3-INP which uses Finite Difference Method (FDM) includes the solution of Poisson equation and particle distribution function. It creates a space charge map during the ray-tracing which give an exact beam trajectories result. This 32-bit version running under extended DOS needs over 128 MB memory on a fast PC for better performance.

2.3 Beam emittance

The beam emittance diagram from an ion source is a must-known property for beam transport system design. To avoid complicated hardwares and destructive properties in many beam emittance measurement devices, a quadrupole scan method has been adopted to this experiment. The method requires only a quadrupole followed by a beam profile monitor. To briefly describe the method, consider a beam phase space diagram and the definition of the beam matrix [33].

$$\sigma = \begin{bmatrix} \sigma_{11} & \sigma_{12} \\ \sigma_{21} & \sigma_{22} \end{bmatrix} = \varepsilon \begin{bmatrix} \beta & -\alpha \\ -\alpha & \gamma \end{bmatrix}, \quad (6)$$

where $\beta, \alpha, \gamma, \varepsilon$ are ellipse parameters, $\alpha = -\beta'$ and $\beta\gamma = (1+\alpha^2)$.

At different positions along the beam transport line the phase ellipse will change its form and orientation, but not its area. The ellipse parameters at any position down stream from the quadrupole are given by

$$\begin{bmatrix} \beta \\ \alpha \\ \gamma \end{bmatrix} = \begin{bmatrix} c^2 & -2sc & s^2 \\ -cc' & (s'c + sc') & -ss' \\ c'^2 & -2s'c' & s'^2 \end{bmatrix} \begin{bmatrix} \beta_0 \\ \alpha_0 \\ \gamma_0 \end{bmatrix}, \quad (7)$$

where $\beta_0, \alpha_0, \gamma_0$ are the ellipse parameters at the entrance of the quadrupole. The transformation matrix elements c, s, c', s' are given by the quadrupole focal length, f and the length L of the drift space between the quadrupole and the beam profile monitor

$$\begin{bmatrix} c & s \\ c' & s' \end{bmatrix} = \begin{bmatrix} 1 & L \\ 0 & 1 \end{bmatrix} \begin{bmatrix} 1 & 0 \\ -1/f & 1 \end{bmatrix} \quad (8)$$

Utilizing the definition of the beam matrix in (6) and $\sigma_{12} = \sigma_{21}$ we get for the determinant

$$\sigma_{11}\sigma_{22} - \sigma_{12}^{2} = \varepsilon^{2}, \tag{9}$$

and the beam sizes at the beam monitor are given by

$$\sigma_{11,monitor} = s^{2}\sigma_{11} + 2sc\sigma_{12} + s^{2}\sigma_{22} \tag{10}$$

By varying the focal length, we measure $\sigma_{11,monitor}$ as a function of the quadrupole strength, *k*. All parameters in (10) are known except for σ_{11}, σ_{12} and σ_{22}.

By fitting these parameters to the measured curve $\sigma_{11,\text{monitor}}(f)$, we can obtain the beam emittance ε from (9). In addition from (6) we can also determine the orientation of the phase ellipse. Thereby, all parameters ($\beta_0, \alpha_0, \gamma_0, \varepsilon$) to design a beam transport line are known.

2.4 Experimental setup

The experimental setup is shown schematically in figure 1. The rf multicusp ion source is a cylindrical chamber made of stainless steel with a diameter of 10 cm and length of 9 cm and is surrounded by 20 columns of Nd-Fe-B magnets. This type of permanent magnet can produce higher B_r than the Sm-Co_5 type. However, it must be well cooled and coated to prevent corrosion from the cooling agent. Figure 2 shows a quarter of the magnetic cusp field lines calculated by the MAGNUS program for Nd-Fe-B and Sm-Co_5 permanent magnets. The cusp field shape looks alike in both cases except the magnetic field strength at the inner chamber wall is higher in the case of Nd-Fe-B magnet with B_r equal to 12.8 kG compared to 9.5 kG for Sm-Co_5. The radial variation of the field for Nd-Fe-B magnet reaches a maximum of 1.8 kG at the chamber wall and decreases exponentially to the source center. The calculations show a nearly field free region (<60 G) in the source center of about 4 cm in diameter in both cases. We expect to get a higher plasma density in this new magnet version. The back plate of the source chamber is attached by 4 rows of the same type of magnets to complete the field line for cusp field continuity. The 13.56 MHz rf power is inductively coupled into the plasma via a two-turn quartz antenna, 6 cm in diameter placed inside the ion source chamber. The antenna is made of a braided copper wire threaded through a quartz tube. A quartz antenna has been found to have a longer lifetime compared to glass or porcelain coated copper antenna [22] and generates a clean Argon plasma compared to the bare copper antenna, which produces high yield of copper atoms from Ar-Cu interaction. The ion source is connected to a 250 l/sec turbomolecular pump and powered by a 1.2 kW rf generator via a matching box. The gas supply is controlled by a MKS mass flow controller Model 1179A and read out by 179A mass flow meter. Experiments have been performed with an Argon flow rate from 1 to 5 sccm at 5-25 mTorr gas pressure range and rf power between 0-500 W unless otherwise specified. The rf power was kept at a maximum of 500 W to prevent overheating of an antenna working in the continuous wave (cw) mode.

The source is characterized in terms of the radial plasma density n(r). The mean free path for electron-neutral collisions in this experiment is in the range between 4-40 cm or longer which is of the order of the source geometry. Long confined electron trajectories due to the line cusp boundaries increase the electron resident time and ionization rate. In the case of an rf discharge, ionization is caused by energetic electron, and so the electron temperature of the plasma is an important factor. In general, the electron temperature depends on the gas pressure as well as the input rf power. One needs to know the electron temperature since in

low-energy ion beams in the 1-10 keV class, ion temperature is the main factor for beam divergence whereas for beam of tens of keV, the non-uniformity of plasma density is the main factor [34]. The measurements have been performed using a self-built movable rf-compensated Langmuir probe. A tungsten cylindrical probe of 150 μm diam with 10 mm length encapsulated in an aluminum sleeve for rf-compensation was used. The probe tip is immersed into the plasma close to the plasma electrode side as shown in figure 1a). The data has been analysed by a Hiden Analytical electrostatic plasma probe model ESP 085 interfaced to a PC.

The extraction system was developed by computer simulations to optimize the electrode geometry. Figure 3 show samples of KOBRA simulations of a 9 keV Argon beam extracted from a triode extraction system following the calculations described above. For the present experiments, the suppressor electrode is mounted 5 mm from the plasma electrode and 2 mm from ground electrode as shown in figure 1b). All electrodes have a 2.5 mm diam hole as the beam exit. The suppressor electrode is biased by a negative potential to control beam optics. During simulations, the perveance was varied from 0.3 P_0 (figure 3a) to 0.45 P_0 (figure 3b) to 1.0 P_0 (figure 3c) to see its influence on the beam optics. It can be observed that for a beam perveance greater or less than 0.45 the beam diverges and is not uniform. The beam in figure 3(b) has a minimum emittance of about 29 mm mrad. In this case, we assume ion temperature equal to 0.1 eV instead of zero to see its effect on beam divergence at low energy extraction.

The emittance measuring equipment in figure 1(b) was constructed based on the quadrupole scan method. It consists of a quadrupole lens and a multiwire beam profile monitor. A quadrupole [35] with a 5 cm aperture and a maximum strength of 5.0 Tesla/m was installed 10 cm from the ground electrode. The beam profile was located 20 cm from the quadrupole. A multiwire profile monitor which has a 3x3 cm^2 active area with 16x16, 150 micron Tungsten sense-wires was a modified version developed by Godfrey et al [36]. The signals from each sense-wire were read out through external multiplexers to a digital storage oscilloscope for beam width determination. An Argon beam was extracted at 9 kV with suppression electrode biased at –500 V and 300 W rf power. To decouple the rf voltage from the extraction voltage, we inserted a 1.2 mH rf choke in series with the dc high voltage supply. This inductor with small stray capacitance functions as a simple L-C low pass filter.

The energy spread of an accelerated beam was measured with the following procedures. The collected ion current as a function of retarding voltage was first measured and the current-voltage (I-V) curve was then differentiated and inversely plotted to determine the energy spread (ΔE) which is defined as the full width at half maximum (FWHM) of the differentiated curve. A self-built retarding field energy analyser [37] has been made for this experiment. The energy spread was measured on an accelerated Argon beam. The assembly is illustrated schematically in figure 1(c). The energy analyser has a 7 cm long and 3 cm diameter grounded metal shield with a 3 mm inlet aperture defining the incoming beam, an electron suppressor for secondary electron suppression and a collector for energy distribution measurements. The collector is connected to a retarding voltage via a 100 kΩ resistor which determines the collected current. The analyser was mounted about 10 cm from the ground electrode of the extraction system. The rf-choke was installed close to the extraction electrode to eliminate the coupling of rf voltage to the dc extracting voltage. The antenna leg between antenna and matching network was well shielded and the rf power supply was operating at the extracting potential to reduce rf coupling to the measurement setup resulting in a large beam energy spread as reported by Lee et al [23].

3. Rf-discharge simulation

The effects of magnetic field to plasma inside the ion source chamber was modeled using a PIC computer code. The X-Windows version of Object-Oriented Particle-in-Cell known as XOOPIC code was chosen for the discharge simulation. XOOPIC version 2.51 is a two-dimensional relativistic electromagnetic particle-in-cell code written in C++ by J.P. Verboncoeur and collaborators at the University of California at Berkeley [38]. The code has also been modified to simulate a laser-plasma interaction in the laser wakefield accelerator [39] and magnetron sputter simulation [40]. The code includes cartesian and cylindrical geometries and can handle electrostatic and electromagnetic simulations for relativistic and non-relativistic particles. It was designed to be user-friendly with a sophisticated graphical user interface (GUI) and an expert system advisor. The particles follow the relativistic equation of motion in electric and magnetic fields then generate a source current for the field equations. The particles are advanced using the relativistic time-center Boris scheme [41]. The code uses a charge conservation current weighting algorithm.

The simulation model for our rf driven multicusp ion source is presented schematically in figure 4. The model is cylindrical axisymmetric 10x9 cm^2 with grid sizes of 32x64 along the r and z space and ideal conducting walls as plasma boundary. The code runs on a Linux server using X11 as X-Windows server. The parameters including Grid, Control, Species, Conductor or Dielectric and Port with generic boundary parameters were set as an input file. The multicusp magnetic field produced by permanent magnets of the ion source is generated by using MS Fortran PowerStation 4.0 to create a table of the field values. The field of each mesh point is then read from the file as specified in the Control group. The field value is similar to that calculated by the MAGNUS code which assumed zero field in ϕ and z axes and so only a radial field exist in the plasma volume. The MCC group for Monte Carlo calculation on particle-particle interaction and particles with background gas was also included. Since it was considered as an inductive discharge, the rf field at 13.56 MHz was launched as a PortTM and ElectrostaticFlag = 0 was added in the Control group to enforce the simulation using the electromagnetic field solver only. The simulations were then carried out with Ar gas pressure of 10 mTorr (MCC group) and an applied rf amplitude of 25 V, equal to a rf power of 500 W at 1.25 ohms antenna impedance (Port group). The secondary electron emission factor from the plasma electrode boundary was set to 0.2 and reduced to 0.1 for the ion source wall boundary with magnetic field (Conductor group). These emission values have to be set to include exact electron fluxes to the plasma generation processes. The time step was as low as 3.0×10^{-12} sec (Control group) and was found to depend very strongly on grid sizes under the Courant limit constraint $c\Delta t < (1/\Delta z^2 + 1/\Delta r^2)^{-1/2}$. The computer running time was more than 3 days for few hundreds nsec simulating time.

4. Results and discussions

4.1 XOOPIC simulation

Typical results of XOOPIC simulation for our ion source geometry are shown in figure 5. In figure 5(a) we plot the calculated particles density with time. Figure 5(b) shows the magnetic field inside the volume due to the input magnetic cusp field distributed in r-z space. Figure 5(c) shows profile of number density of electron in r-z space where figure 5(d) shows that of Argon. All profiles were acquired after 373 nsec which is about five times the radio frequency period. These profiles seem to be stable after the elapsed time, in which the

system could be considered as approaching the steady state. Starting with an initial particle density of 10^{16} m^{-3}, the density in the field free zone grew at least two orders of magnitude to 10^{18} m^{-3}. Due to the limited time range, the actual steady state is not yet reached and it can be seen that the number of particles represented in figure 5(a) continuing to increase exponentially. The magnetic field inside the source chamber in figure 5(b) has the effect of an added localized field due to the rf-induction over the field free region. In this simulation, it is shown that the localized field in the field free zone is less than 0.015 Tesla. The particle density in r-z space as shown in figure 5(c) and (d) is distributed uniformly along the entire radial axis except near the edge where a strong magnetic field exists. Electrons are clearly seen to be confined in the field free zone. In a simulation without a magnetic field the particle density was found to be non-uniform along the radial axis with very poor plasma density. Moreover, the average kinetic energy of electrons is much lower in the case of magnetic confinement. Figure 5(e) and (f) give a clearer picture of the particle distribution for electron and Argon in r-z space, respectively. It can be distinctly seen that the electron density near the magnetic wall has been significantly affected by the strong magnetic field much more than that of Argon which is heavier. The distorted distribution near the antenna may be due to a high fluctuation of an induced rf field direction along the z-axis which can be seen from the E-field plot (not shown here). This causes a distorted Poynting vector because the plasma-rf power absorption near this region is probably not uniform. Even though, the number of particles in 5(a) did not yet reach a steady state, the graph of electron temperature T_e against time in figure 5(g) approaches a stable value with an average T_e of about 10 eV.

4.2 Electron temperature, plasma uniformity and density

The plasma density profile was measured along the radial direction for a 9 cm source (figure 6). The density profile is fairly uniform (+/- 8 %) within the plasma diameter of 6 cm then decreases rapidly at the source wall. Such a distribution could be attributed to the magnetic cusp fields which confines electrons in the plasma region. Compared with the measurement of Menard et al [42] our uniformity variation is about 2 % higher due to a well known behavior that plasma uniformity variation reduces at low operating pressure. Also, our experiment indicates less uniformity of Ar gas than diatomic gas like H_2 or N_2 as observed by others [42] under the same gas pressure. For a N_2 pressure at 8 mTorr with P_{rf} = 200 W, the non uniformity was only about 2 %. This difference in uniformity could be due to the availability of multiple long-lived excited energy states of neutral diatomic gas. It can be seen from simulation results in figure 5(c) and (d) that electron and Argon densities are less uniform near the antenna which may be due to higher flux of the nearby azimuthal electric fields. From the same figures we can also see that plasma confinement due to the multicusp field is similar to the measurement made after a few rf cycles.

The plasma density of up to 1.5 x 10^{18} m^{-3} can be obtained at 500 W rf power. In comparison with the simulated results, we can see that the plasma density reaches and remains at a value of 10^{18} m^{-3} almost instantly after a few rf cycles. Figure 7 illustrates the variations of the electron temperature T_e against the base pressure at 200 W. The electron temperature (1-3 eV) is found to be relatively independent of the source radius and slightly increases with rf power. The higher electron temperature at a rf power below 200 W is due to a transition from capacitive coupling to inductive coupling. Our results also agree with other experiments [43,44] for linear decreasing of T_e as a function of log P for cylindrical inductive discharge. We did not measure T_e at lower pressure due to an unignitable condition as mentioned in the previous work [24]. We also note that our T_e value is much lower than that predicted by the

XOOPIC calculation. The peak pressure for maximum discharge efficiency for this geometry and rf frequency is around 8 mTorr. We used this value of pressure through the whole measurement. Compared with our previous measurement [24], the current density of Ar increases from 29 mA/cm^2 in Sm-Co_5 version to 36 mA/cm^2 for this version at the same Argon pressure even though there is no significant difference in the field free region of our sources using different type of permanent magnets as indicated in figure 2. This 20 % increase in plasma density for the Nd-Fe-B magnet version is considered significant for our application. In addition, the need to use a filter magnet for separating the excitation and extraction region in this range of rf excitation power may not be necessary because of the low value of T_e as our measurement indicates.

4.3 Beam emittance

The beam emittance was measured with a quasi-Pierce type extracting system consisting of the three stainless-steel electrodes with 5 and 2 mm spacing and a 2.5 mm diam exit hole. All sharp edges have been removed to enhance beam quality as reported before by Reijonen et al [45]. From the beam width measurement with the beam profile monitor as a function of quadrupole strength, beam parameters can be derived. Figure 8 shows a typical phase space diagram of the emitted beam which is diverging.

The rms emittance ε = 32 +/- 4 mm mrad which is consistent with the KOBRA calculations in figure 3(b). From the calculation, about 86 % of the beam particles are in the phase-space ellipse. These calculations optimize the extracting system for an Argon density varying from 25 to 75 mA cm^{-2} and the rms emittance is found to vary between 28 and 48 mm mrad at 9 kV extraction. Thus measurement also provides information on the beam size, x = $(\varepsilon\beta)^{1/2}$ = 6 mm and the beam divergence, x' = $(\varepsilon\gamma)^{1/2}$ = 12 mrad at the entrance to the quadrupole. The uncertainty in this measurement is mainly due to wire spacing of the beam profile monitor and polynomial fitting. The emittance of our ion source is fairly small compared to the value of 200-400 mm mrad as measured in an rf ion source by Abdelaziz et al [46]. Expressed in term of normalized rms emittance defined by $\varepsilon_n = (2V/mc^2)^{1/2}\varepsilon$, where V is an accelerating voltage, it is found to be only 0.02 π mm mrad compared to 0.04 π mm mrad in double electrode extracting system measured by Leung et al [2] for an Argon beam. It should be noted that Leung et al used a different type of emittance measuring device (electrostatic, slit to slit or Allison type emittance scanner) and a double electrode extracting system. Also, they measured the emittance at higher rf power.

4.4 Beam energy spread

At 200 W rf power and 4 kV extracting voltage, the energy spread is found to be 3.6 +/- 0.5 eV at 8 mTorr gas pressure. Our measurements indicate that the energy spread depends on the extracting voltage as shown in figure 9. This voltage dependence has been reported by Kuo et al [47]. The high fluctuation of the energy spread at low extracting voltage may be due to an rf interference and the stability of the dc power supply itself. The measurement became much more stable when the extracting voltage exceeds 2 kV. The energy spread has been found to decrease from 4.8 eV to 3.4 eV as the gas pressure increases to 25 mTorr at 500 V extraction. The variation of the energy spread with gas pressure is attributed to the fall of plasma potential which was observed to decrease from 9 to 7 V when the Argon pressure increases from 8 to 25 mTorr. Figure 10 shows an effect of introducing a 0.1 μF bypass capacitor while the rf choke is still installed. The added capacitor reduced the beam current. This effect may be explained as a reduction of high voltage by a high capacitive load resulting

in a reduction of extractable beam current. We note that without an rf choke, the energy spread goes up to 5 eV +/-1.5 eV. The rf choke functions as a low pass filter which is effective in eliminating the modulation of the dc acceleration voltage with rf interference.

5. Conclusions

The characteristics of a 13.56 MHZ rf driven multicusp ion source have been studied. Replacing the more expensive Sm-Co_5 permanent magnet with a 30 % stronger field Nd-Fe-B magnet results in an increase in plasma density of about 20 %. The simulated results by the code XOOPIC for plasma distribution and density at 373 nsec indicate the need of a multicusp magnetic field which is supported by results from the Langmuir probe measurements. This type of ion source can deliver plasma density up to 1.5 x 10^{18} m^{-3} at 500 W rf power uniformly distributed over the radial axis to within 8 %. The rms emittance at 9 kV extracting voltage is measured to be 32 +/- 4 mm mrad. The accelerated Argon axial beam energy spread have been observed to vary from 3 to 5 eV for an extracting voltage decreasing from 4 to 0.5 kV.

The use of only an rf-choke of 1.2 mH, instead of an expensive high voltage capacitor to function as a low pass filter, in series with the extraction dc power supply can eliminate the interference from the rf voltage in this range of rf power which results in a reduction of an axial beam energy spread. This 13.56 MHz rf driven multicusp source has proven not only capable of high density Argon beam production but also useful in generating a broad uniform Argon beam. Design and experiments of a beam transport system for Argon micro milling are in progress and results will be reported in near future.

Acknowledgements

We would like to thank K.N. Leung of LBNL for his guidance and assistance in the early phase of this project. We thank J. Engemann of FMT for his useful discussion on the design of the retarding field energy analyser, J.P. Verboncoeur of UCB for his helpful suggestion on running the XOOPIC simulation, and to H. Wiedemann of SLAC for his valuable advice on the emittance measurements and N. Tondee for performing the measurements. This work was supported by the Thailand Research Fund.

References

1. Wells S.B., Takeiri Y., Newman A.F., McAdams R., and Holmes A.J.T. 1992 Rev. Sci. Instrum. **63** 2735
2. Wutte D., Freedman S., Gough R., Lee Y., Leitner M., Leung K.N., Lyneis C., Pickard D.S., Williams M.D. and Xie Z.Q. 1998 Nucl. Instr. and Meth in Phys. Res. B **142** 409
3. Lee Y., Leung K.N. and Williams M.D. 1999 Proc. of the 1999 Particle Accelerator Conference (New York, 1999) p 2575
4. Burns E.J.T., and Bischoff G.C. 1997 Application of Accelerators in Research and Industry, (New York, AIP Press) 1207
5. Limpaecher R. and MacKenzie K.R. 1973 Rev. Sci. Instrum. **44** 726
6. Leung K.N., Samec T.K. and Lamm A. 1975 Phys. Letters **51A(8)** 490
7. Leung K.N., Collier R.D., Marshall L.B., Gallaher T.N., Ingham W.H., Kribel R.E. and Taylor G.R. 1978 Rev. Sci. Instrum. **49(3)** 321
8. Leung K.N. and Keller R. 1990 Rev. Sci. Instrum. **61** 333
9. Zakhary G. 1995 Rev. Sci. Instrum. **66** 5419

10. Sarstedt M., Lee Y., Leung K.N., Perkins L.T., Pickard D.S., Weber M., and Williams M.D. 1996 Rev. Sci. Instrum. **67** 1249
11. Shirakawa T. Toyoda H. and Sugai H. 1990 Jpn. J. Appl. Phys. **29(6)** L1015
12. Suanpoot P., Boonyawan D., Rhodes M. and Vilaithong T. 1998 J. Plasma Fusion Res. SERIES, Vol. **1** 526
13. Lister G.G., and Cox M. 1991 Plasma Sources Sci. Technol. **1** 67
14. Piejak R.B., Godyak V.A., and Alexandrovich B.M. 1992 Plasma Sources Sci. Technol. **1** 179
15. Keller J.H. 1996 Plasma Sources Sci. Technol. **5** 166
16. Kolobov V.I., and Economou D.J. 1997 Plasma Sources Sci. Technol. **6** R1
17. You K.I., and Yoon N.S. 1999 Physical Rev. E **59(6)** 7074
18. Zorat R., Goss J., Boilson D., and Vender D. 2000 Plasma Sources Sci. Technol. **9** 161
19. Suzuki K., Nakamura K., Ohkubo H., and Sugai H. 1998 Plasma Sources Sci. Technol. **7** 13
20. Gudmundsson J.T. 2001 Plasma Sources Sci. Technol. **10** 76
21. Lee Y., Gough R.A., Kunkel W.B., Leung K.N., Perkins L.T., Pickard D.S., Sun L., Vujic J., Williams M.D., Wutte D., Mondelli A.A. and Stengl G.1997 Nucl. Instr. and Meth in Phys. Res. A **385** 204
22. Lee Y., Gough R.A., Leung K.N., Perkins L.T., Pickard D.S., Vujic J., Wu L.K., Olivo M. and Einenkel H. 1998 Rev. Sci. Instrum. **69(2)** 1023
23. Lee Y., Gough R.A., Kunkel W.B., Leung K.N., Perkins L.T., Pickard D.S., Sun L., Vujic J., Williams M.D. and Wutte D. 1997 Rev. Sci. Instrum. **68** 1398
24. Boonyawan D., Suanpoot P., and Vilaithong T. 1999 Surf. Coat. Technol. **112** 314
25. Bruenger W.H., Torkler M. Leung K.N., Lee Y. Williams M.D. Loeschner H., Stengl G., Fallmann W., Paschke F., Stangl G., Rangelow I.W. and Hudek P. 1999 Microelectronic Engineering **46** 477
26. Lee Y., Gough R.A., King T.J., Ji Q., Leung K.N., McGill R.A., Ngo V.V., Williams M.D., and Zahir N. 1999 Microelectronic Engineering **46** 469
27. Scipioni L., Stewart D., Ferranti D., and Saxonis A. 2000 J. Vac. Sci. Technol. B18(6) 3194
28. Libermann M.A. and Lichtenberg A.J. 1994 Principles of Plasma Discharges and Material Processing (New York: John Wiley & Son)
29. Zhang H.1999 Ion Sources (Berlin: Springer) p206
30. MAGNUS, 1987 A Three-Dimensional Non-Linear Magnetostatic, Computer Program (FL: Ferrari Associates, Inc.)
31. Shubaly M.R. 1987 Nucl. Instr. and Meth in Phys. Res. B **26** 195
32. KOBRA3-INP Manual 1999 Spedtke P. INP, Germany
33. Strehl P. 1995 Handbook of Ion Sources (New York: CRC Press) p437
34. Ishikawa J. 1998 Rev. Sci. Instrum. **69** 863
35. Junphong P. 1999 M.S. Thesis, Chiang Mai University
36. Godfrey L., Hoyes G.G. and Pairsuwan W. 1990 Nucl. Instrum. and Meth. B **51** 294
37. Engemann J. 2000 Private communications.
38. Verboncoeur J.P., Langdon A.B. and Gladd N.T. 1995 Comp. Phys. Comm. **87** 199
39. Giaconne R.E., Cary J.R., Bruhwiler D., Mardahl P.and Verboncoeur J.P. 2000 Proc. 7th European Particle Accelerator Conference (Vienna, 2000) p907
40. Shon C.H., Lee J.K., Lee H.J., Yang Y. and Chung T.H. 1998 IEEE Trans. on Plasma Science **26 (6)** 1635
41. Birdsall C.K. and Langdon A.B. 1991 Plasma Physics via Computer Simulation (Bristol: Adam Hilger).
42. Menard J. and Intrator T. 1996 Plasma Sources Sci. Technol. **5** 363
43. Gudmundsson J.T., and Lieberman M.A. 1997 Plasma Sources Sci. Technol. **6** 540
44. Yang J.G., Yoon N.S., Kim B.C., Choi J.H., Lee G.S., and Hwang S.M. 1999 IEEE Trans. on Plasma Science **27(3)** 676
45. Reijonen J., Heikkinen P., Liukkonen E. and Arje J. 1998 Rev. Sci Instrum. **69** 1138
46. Abdelaziz M.E., Zakhary S.G., and Ragheb M.S. 2000 Rev. Sci. Instrum. **71** 1137

47. Kuo T., Yuan D., Jayamanna K., McDonald M., Baartman R., Mackenzie G., Bricault P., Dombsky M., Schmor P., Dutto G., Lee Y., Leung K.N., Williams D., and Gough R. 1998 IEEE Trans. on Plasma Science 2675

Figure captions

Figure 1 Schematic diagram of the experimental setup: (a) rf driven multicusp ion source working at 13.56 MHz and rf compensated Langmuir probe; (b) emittance measuring devices; and (c) retarding field energy analyser

Figure 2 The calculated cusp magnetic fields for Nd-Fe-B and Sm-Co_5 magnets. The measured field at the source wall is 1.8 kG for Nd-Fe-B and 1.2 kG for Sm-Co_5.

Figure 3 Samples of KOBRA simulation of 9 keV Argon beam from a triode extraction system at different perveance: (a) 0.3 P_0; (b) 0.45 P_0; and (c) 1.0 P_0

Figure 4 Schematic diagram of the cylindrical ion source used in the XOOPIC simulation. The *z*-axis is taken as the symmetry axis.

Figure 5 XOOPIC simulation results in r-z space at 10 mTorr base pressure: (a) the calculated particles density against time; (b) the magnetic field inside the source volume; (c) profile of the electron density; (d) profile of the ion density; (e) electron distribution; (f) ion distribution; and (g) T_e profiles against time. All data are taken at 373 nsec revolution time

Figure 6 Radial density profile of Argon and Nitrogen plasmas measured at $z = 8$ cm, for 200 W rf power, 8 mTorr base pressure.

Figure 7 Radial electron temperature as a function of base pressure for 200 W Argon plasma.

Figure 8 Phase space diagram of the emitted Argon beam.

Figure 9 Axial energy spread as a function of extracting voltage for 200 W, 8 mTorr Argon plasma.

Figure 10 Effect of introducing a 0.1 uF bypass capacitor on the energy spread curve.

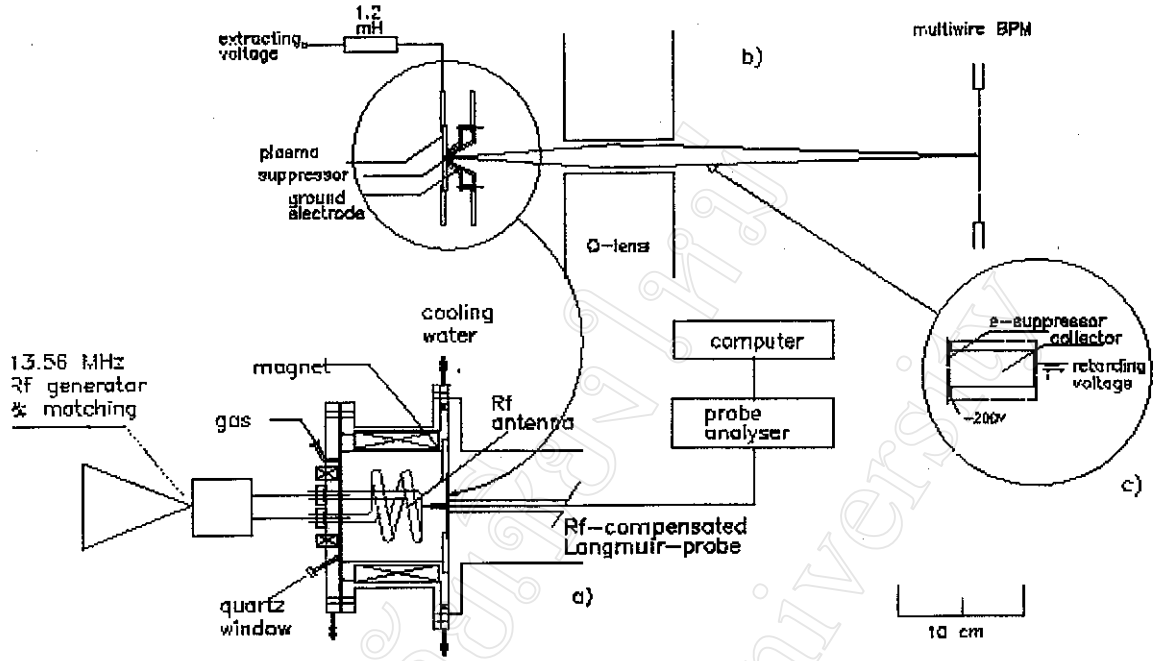
1.2 mH
extracting voltage
b)
multiwire BPM
plasma
suppressor
ground electrode
Q-lens
cooling water
computer
e-suppressor
collector
retarding voltage
-200V
13.56 MHz
RF generator
& matching
magnet
gas
Rf antenna
probe analyser
c)
Rf-compensated Langmuir-probe
a)
quartz window
10 cm

1)

2)

3)

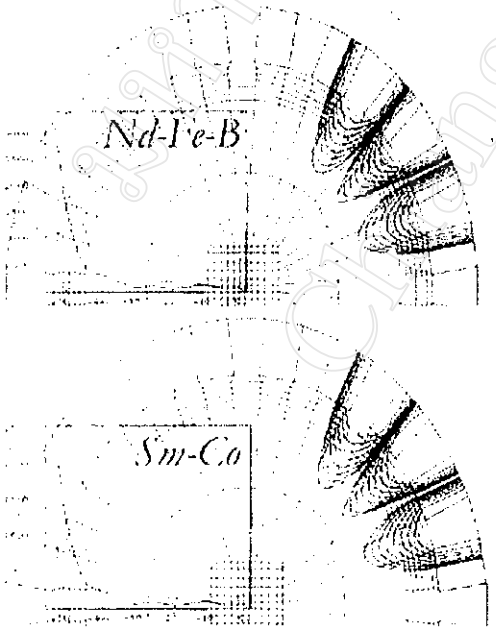
Nd-Fe-B
Sm-Co

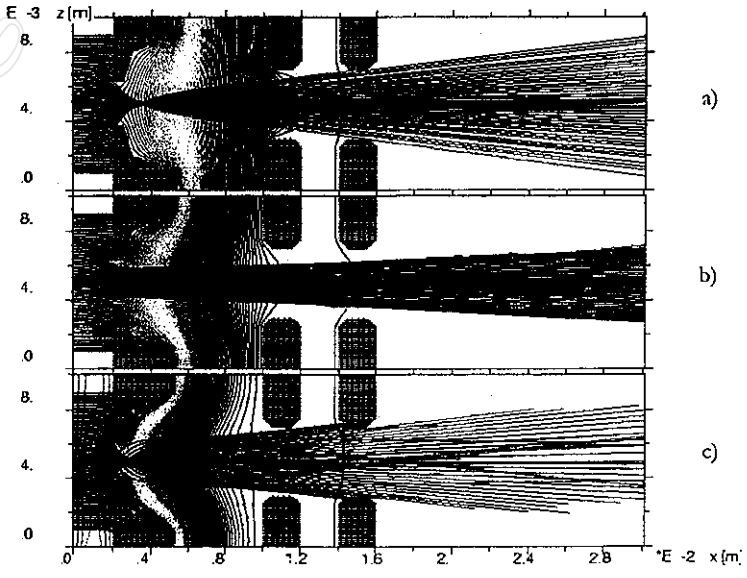
E -3 z[m]
8.
4.
.0
8.
4.
.0
8.
4.
0
a)
b)
c)
0
.4
.8
1.2
1.6
2
2.4
2.8
*E -2 x[m]

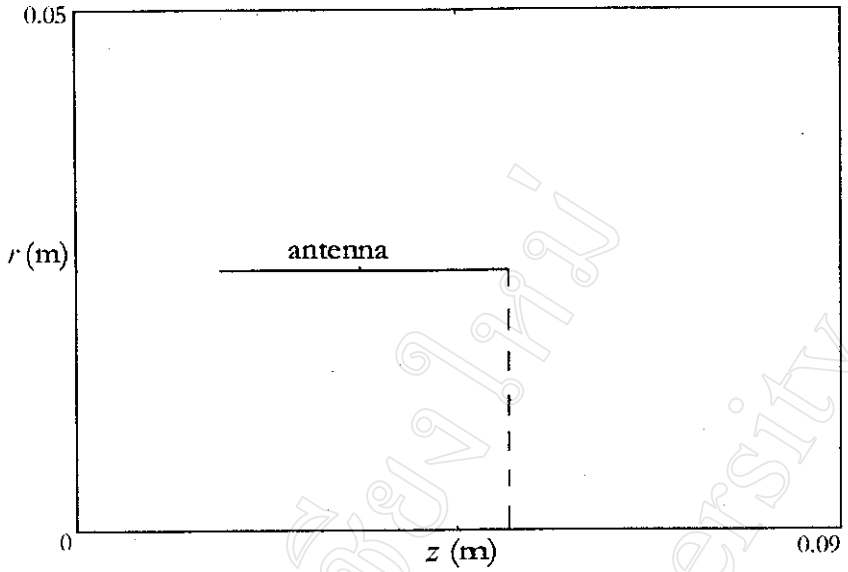

4)

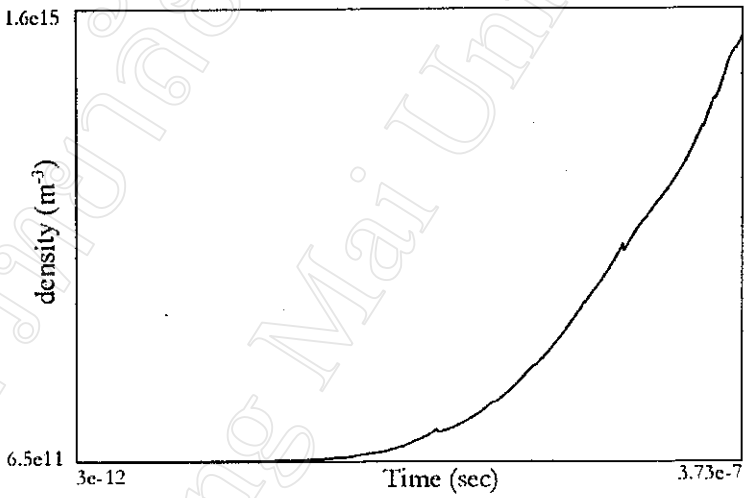

5(a)

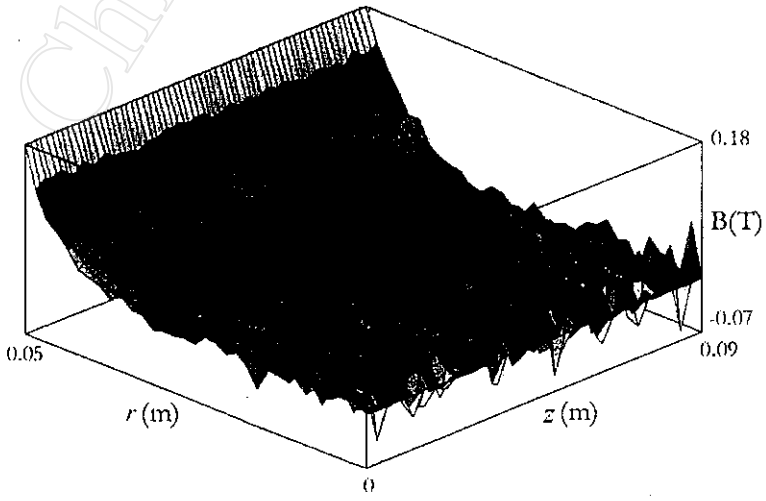

5(b)

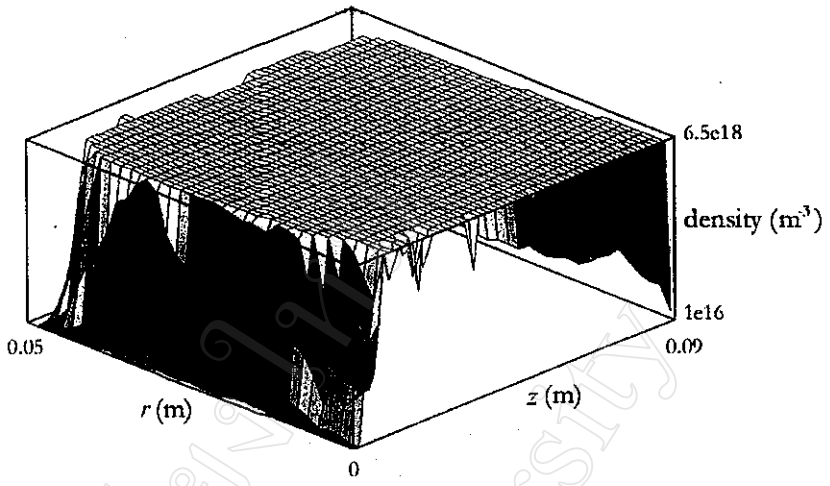
6.5e18
density (m^{-3})
1e16
0.05
0.09
r (m)
z (m)
0

5(c)

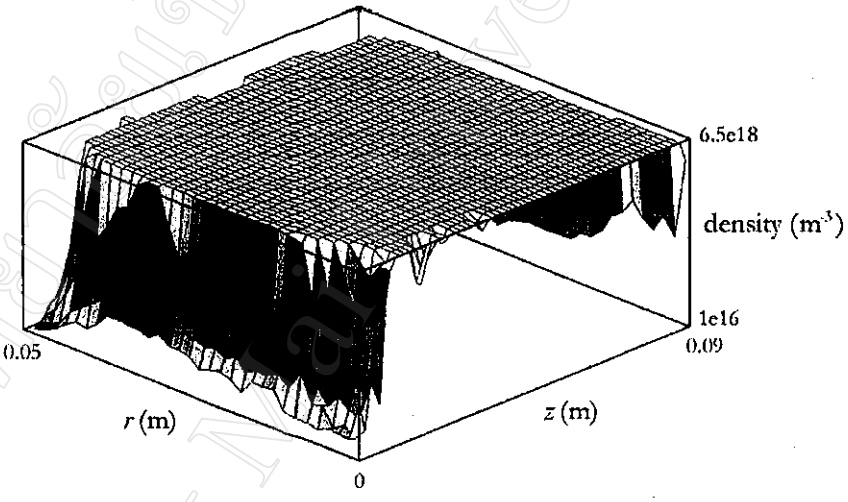
6.5e18
density (m^{-3})
1e16
0.05
0.09
r (m)
z (m)
0

5(d)

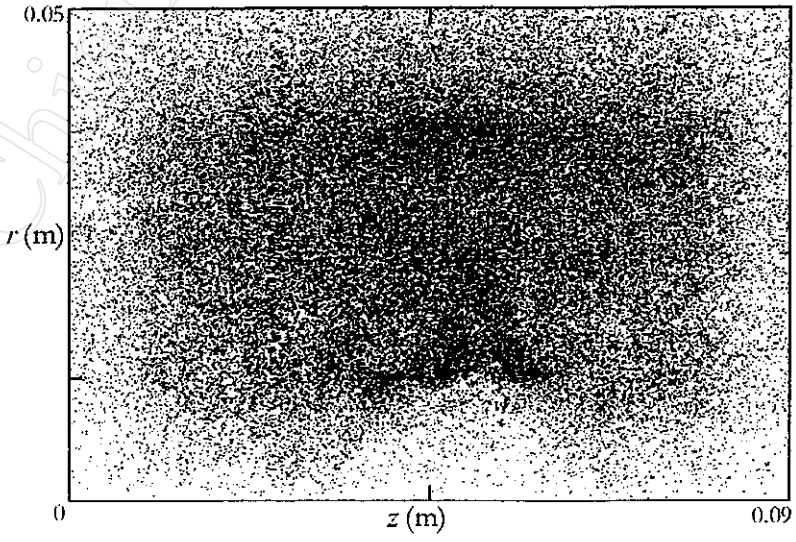
0.05
r (m)
0
z (m)
0.09

5(e)

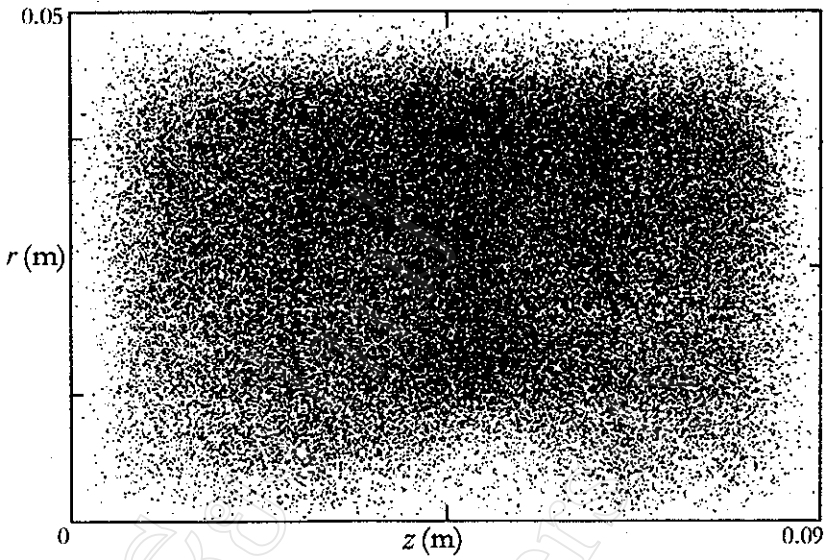

5(f)

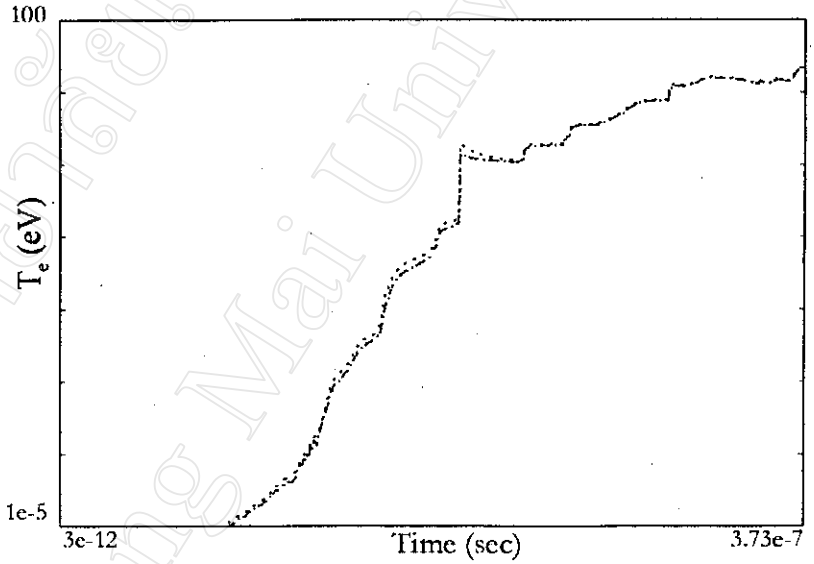

5g)

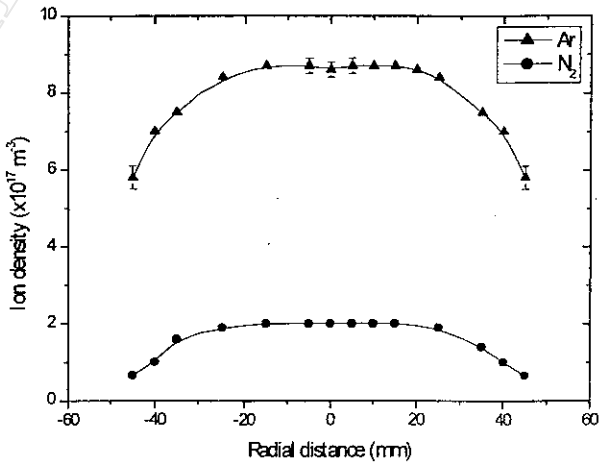

6)

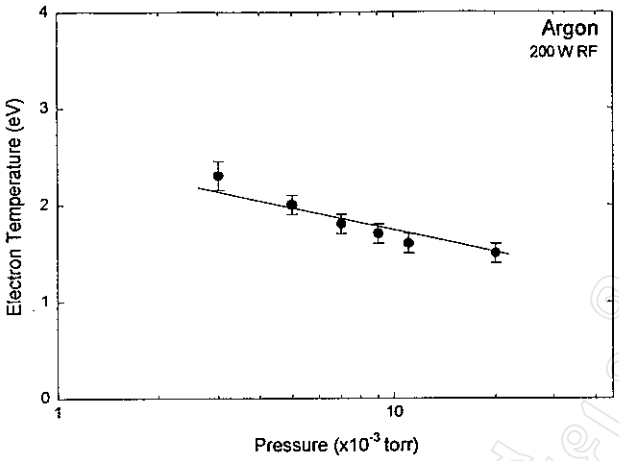

7)

8)

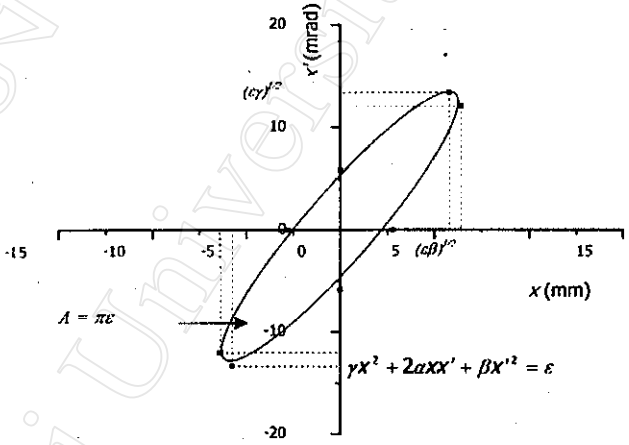

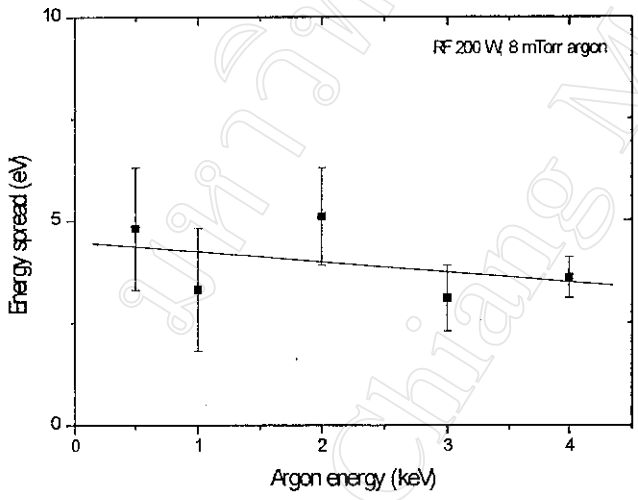

9)

10)

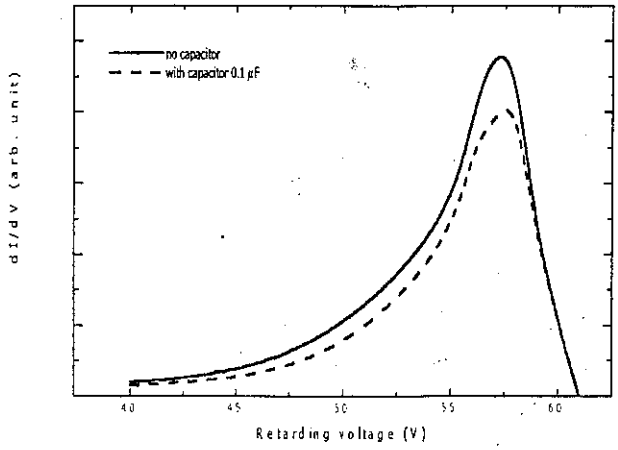

CIRRICULUM VITAE

Name Mr. Dheerawan Boonyawan

Birth date 21 September 1965

Education

Year	Institution	Degree	Field
1982-1986	Chiang Mai University	B.S.	Physics
1987-1989	Chiang Mai University	M.S.	Physics

Training and Fellowship

Year	Institution	Field
1989	Chiang Mai University, Thailand	Nuclear Physics
1991	Shianghai University, China	E- Beam Irradiation
1998	University of Wuppertal, Germany	Plasma Physics